Report

Cell Reports

Macrophages Regulate Schwann Cell Maturation after Nerve Injury

Graphical Abstract

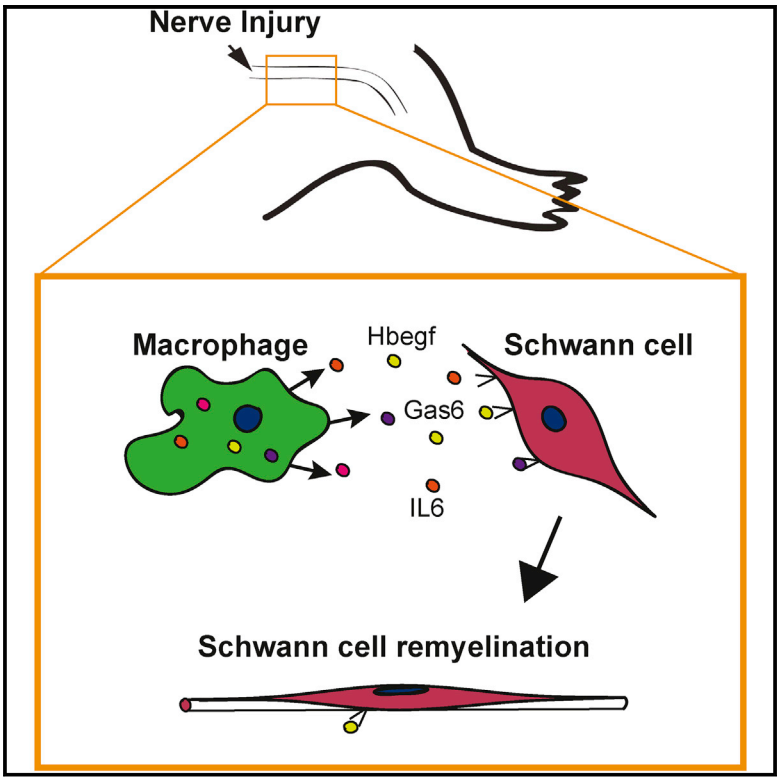

Authors

Jo Anne Stratton, Alexandra Holmes, Nicole L. Rosin, ..., Tuan Trang, Rajiv Midha, Jeff Biernaskie

Correspondence

jeff.biernaskie@ucalgary.ca

In Brief

Stratton et al. demonstrate that macrophages persist in the injured rodent and human nerve and regulate Schwann cells. Macrophages have a unique transcriptional profile, including the expression of Gas6, that functions to regulate Schwann cell remyelination.

Highlights

- Macrophages persist in the injured nerve in rodents and humans
- Macrophages regulate Schwann cells and conduction velocity post-injury
- Macrophages in the injured nerve have a complex transcriptional profile
- Macrophage-derived Gas6 regulates Schwann cell maturation

Stratton et al., 2018, Cell Reports *24*, 2561–2572
September 4, 2018
https://doi.org/10.1016/j.celrep.2018.08.004

CellPress

Cell Reports
Report

Macrophages Regulate Schwann Cell Maturation after Nerve Injury

Jo Anne Stratton,[1,2,3] Alexandra Holmes,[1,2] Nicole L. Rosin,[2] Sarthak Sinha,[2] Mohit Vohra,[1,4] Nicole E. Burma,[1,2] Tuan Trang,[1,2] Rajiv Midha,[1,4] and Jeff Biernaskie[1,2,3,5,*]

[1]Hotchkiss Brain Institute, University of Calgary, Calgary, AB T2N 4N1, Canada
[2]Department of Comparative Biology and Experimental Medicine, Faculty of Veterinary Medicine, University of Calgary, Calgary, AB T2N 4Z6, Canada
[3]Alberta Children's Hospital Research Institute, University of Calgary, Calgary, AB T2N 4N1, Canada
[4]Department of Clinical Neurosciences, Cumming School of Medicine, University of Calgary, Calgary, AB T2N 4Z6, Canada
[5]Lead Contact
*Correspondence: jeff.biernaskie@ucalgary.ca
https://doi.org/10.1016/j.celrep.2018.08.004

SUMMARY

Pro-regenerative macrophages are well known for their role in promoting tissue repair; however, their specific roles in promoting regeneration of the injured nerve are not well defined. Specifically, how macrophages interact with Schwann cells following injury during remyelination has been largely unexplored. We demonstrate that after injury, including in humans, macrophages function to clear debris and persist within the nerve microenvironment. Macrophage ablation immediately preceding remyelination results in an increase in immature Schwann cell density, a reduction in remyelination, and long-term deficits in conduction velocity. Targeted RNA-seq of macrophages from injured nerve identified Gas6 as one of several candidate factors involved in regulating Schwann cell dynamics. Functional studies show that the absence of Gas6 within monocyte lineage cells impairs Schwann cell remyelination within the injured nerve. These results demonstrate a role for macrophages in regulating Schwann cell function during nerve regeneration and highlight a molecular mechanism by which this occurs.

INTRODUCTION

In trauma patients, 2.8% present with peripheral nerve injury (PNI) (Noble et al., 1998) and those with severe cases often suffer from chronic pain and permanent disability (Siemionow and Brzezicki, 2009), with limited effective treatment. Pro-regenerative macrophages are well known for their role in orchestrating tissue repair and remodeling. They are active participants in bone remodeling, hair follicle regeneration, and CNS remyelination (Miron et al., 2013; Gordon and Plüddemann, 2017; Wang et al., 2017). Although depletion of macrophages following peripheral nervous system injury impairs regeneration and results in worsened outcomes (Barrette et al., 2008), the identity and the extent of their contribution to the regenerative process remain unclear (Stratton and Shah, 2016). Schwann cells are the primary glial cells within the peripheral nervous system (PNS), and their unique capacity to dedifferentiate, re-enter the cell cycle, and subsequently remyelinate regenerating axons makes them an essential player in nerve regeneration (Mirfeizi et al., 2017). Prior evidence suggests that macrophages interact with Schwann cells, including the regulation of migration, mitosis, and dedifferentiation (Cattin et al., 2015; Chen et al., 2015; Martini et al., 2008; Stratton et al., 2016), but whether they regulate remyelination, the final regenerative phenotype that many Schwann cells elicit, is unclear.

In this study, we use rodent models of nerve injury to decipher the role of macrophages in nerve regeneration. We demonstrate that following nerve injury, macrophages clear debris and persist long term post-injury. By depleting macrophages, we demonstrate that they are essential for successful regeneration. We describe the transcriptional profile of macrophages within the injured nerve and identify several macrophage-derived ligands that influence Schwann cell phenotype. We demonstrate that one of these ligands, Gas6, promotes Schwann cell differentiation and remyelination of regenerating axons. Finally, we confirm that macrophages also persist within denervated human nerves and express low levels of Gas6, suggesting that its levels may be modulated therapeutically to promote remyelination by activating endogenous Schwann cells.

RESULTS

After Nerve Injury, Marrow-Derived Macrophages Persist for Several Weeks and Are Found in Close Association with Schwann Cells during Maturation and Remyelination

To establish the source of macrophages and further define their spatiotemporal dynamics in relation to Schwann cells following injury, we assessed injured nerves across several time points using immunohistochemistry (Figure 1). First, we assessed the presence of monocyte-derived macrophages using a GFP-tagged bone marrow transplant approach (Figure 1A). We found that there were minimal numbers of GFP-tagged cells in uninjured nerves but that post-injury, GFP^+ cells dominated the nerve and persisted at the injury site for at least 16 weeks (Figures 1B and 1C). Only 24.0% ± 5.5%–36.6% ± 2.6% of total macrophages (Iba1+ cells) were GFP negative, suggesting that most

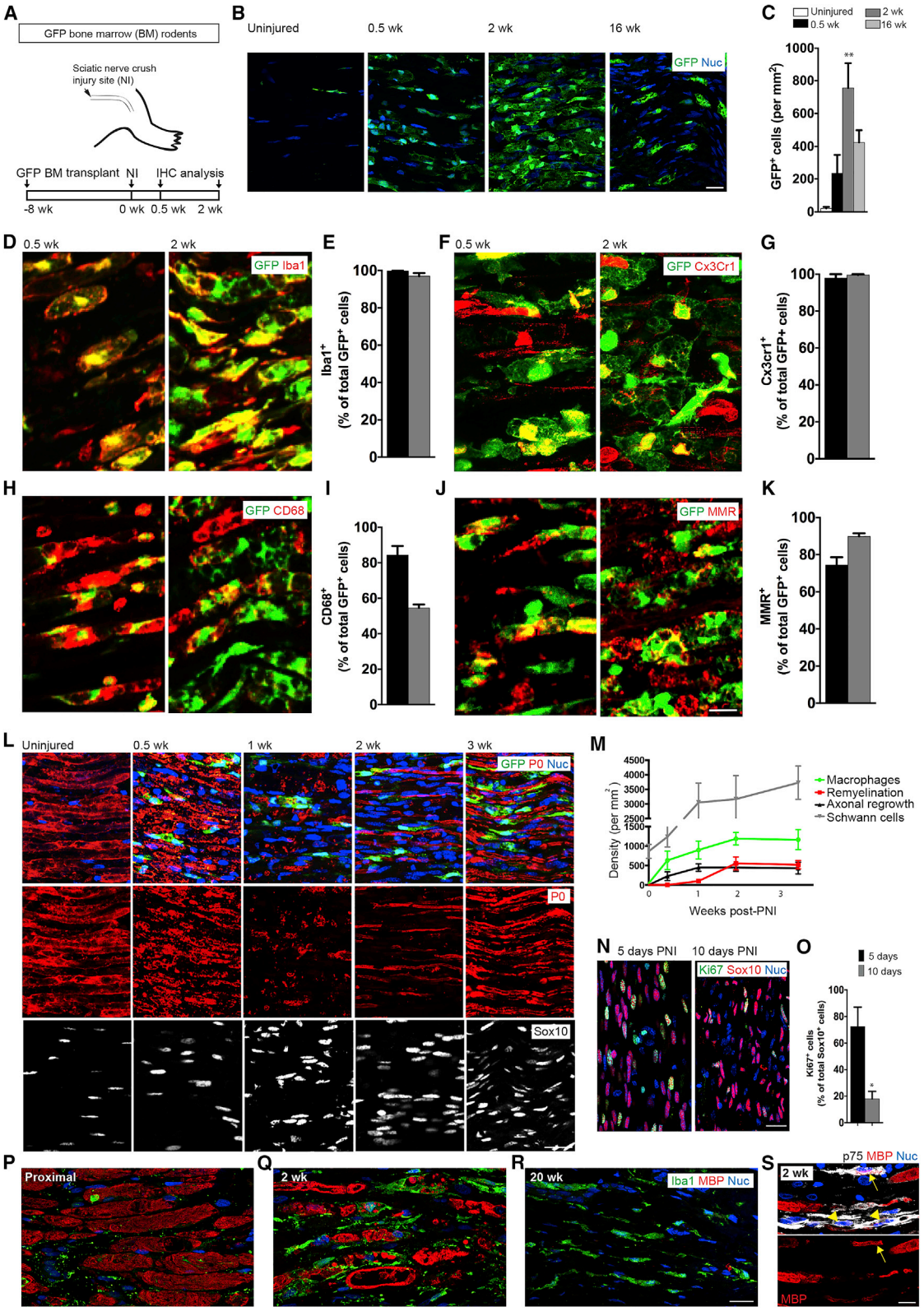

(legend on next page)

macrophages present were derived from infiltrating GFP$^+$ monocytes that entered the injury site. Of these hematogenous monocyte-derived macrophages, most expressed classic macrophage-associated proteins, such as Iba1 and CD68, but also expressed proteins associated with an anti-inflammatory macrophage profile, such as the Mannose receptor (MMR) and the Cx3 chemokine receptor 1 (Cx3cr1) at both 0.5 and 2 weeks after nerve injury (Figures 1D–1K). Next, we assessed the spatial and temporal relationships of these cells to Schwann cells. We found a sharp increase in Schwann cell numbers between 0.5 and 1 week post-injury—time points at which macrophages were also starting to dominate the nerve and clear debris (Figures 1L and 1M). Schwann cell numbers largely plateaued between 1 and 2 weeks, correlating with a reduction in Schwann cell proliferation within the 2nd week compared to the 1st week post-injury (Figures 1N and 1O). By 2 weeks, thin myelin segments were apparent, with macrophages found in close association with these segments and segments becoming thicker by 3 weeks post-injury (Figure 1L).

Following Chronic Denervation in Human Nerve Injury, Macrophages Persist at the Injury Site for Months Post-injury

To assess macrophage dynamics in human nerve injury, we assessed acute and chronic nerve injury samples collected at 2 weeks and 5 months post-injury, respectively (Figures 1P–1S). At 2 weeks post-injury, there was limited immunoreactivity for Iba1$^+$ macrophages in nerve tissue proximal to the injury site (Figure 1P). Instead, we found widespread phagocytic myelin-laden macrophages (Iba1$^+$ MBP$^+$) throughout the nerve distal to the injury site (Figure 1Q), consistent with what we observed following injury in rodents (Figure 1L). By 5 months post-injury, macrophages remained in the distal stump, although myelin debris was already cleared. We observed rare instances of thin MBP$^+$ myelin segments, often in close association with p75$^+$ Schwann cells (Figure 1S), suggesting at least some attempt of remyelination by dedifferentiated Schwann cells.

Macrophage-Secreted Factors Are Potent Regulators of Schwann Cell Function

We used an *in vitro* approach to determine whether macrophages could influence Schwann cells via secreted factors (Figures 2A–2E). After initially plating Schwann cells in proliferation-supportive conditions (+neuregulin), conditioned media (CM) from macrophages, fibroblasts, or Schwann cells was added. After 48 hr, there were 46.7% more Schwann cells in the media control group compared to the macrophage CM group (Figures 2A–2C) ($p < 0.01$). Consistent with this, there were more proliferative Schwann cells in the media-alone group versus the macrophage CM group (Figures 2A and 2D) ($p < 0.01$). Relative to macrophage CM, there were no notable differences detected following fibroblast or Schwann cell CM treatment compared to media alone in either Schwann cell number or proliferation. In addition, there were no differences in the expression of the mature Schwann cell protein P0$^+$ across all groups (Figure 2E).

Deficiency of Macrophages Results in an Aberrant Schwann Cell Response, Compromised Remyelination, and Impaired Conduction Velocity after Nerve Injury

Given the pronounced effect of macrophage CM on isolated Schwann cells and our *in vivo* observation showing a sustained presence of macrophages in remyelinated segments at 2 weeks post-injury (Figures 1L and 1M), we hypothesized that macrophages play a role in regulating Schwann cell dynamics during the (sub-acute) regenerative stage following nerve injury *in vivo*. To test this hypothesis, we used mannosylated liposomes containing clodronate to ablate macrophages beginning at 1 week post-injury (Figure 2F). We detected the uptake of control, non-clodronate-containing, fluorescent-tagged mannosylated liposomes in most debris-laden macrophages cells, but not

Figure 1. Following Nerve Injury, Bone Marrow-Derived Macrophages Persist for Several Weeks and Are Found in Close Association with Schwann Cells at Several Stages during Schwann Cell Maturation

(A) Experimental design. Immunohistochemical analysis of nerve injury at 0.5 and 2 weeks post-injury was performed in rodents with GFP-tagged bone marrow. Two months before injury, wild-type rodents were irradiated and then received a tail vein injection of 1 million GFP+ bone marrow cells.

(B and C) Representative immunohistochemical images demonstrated minimal numbers of GFP-tagged cells (green) in uninjured nerves, but post-injury, these cells dominated the nerve and persisted at the injury site for several weeks (B). This observation was also reflected in quantification (C). n = 3 per time point; **p = 0.001 versus uninjured. Error bars indicate ± SEM. Scale bar, 20 μm.

(D–K) Representative immunohistochemical images demonstrated that most GFP-tagged cells (green) expressed macrophage-associated proteins (red) (D, F, H, and J), including MMRs and Cx3cr1—both receptors associated with an anti-inflammatory macrophage profile. These observations were also reflected in quantification, in which anywhere from 54.6% ± 1.9% to 99.7% ± 0.1% of GFP$^+$ cells were observed to express these 4 markers (E, G, I, and K). Only 24.0% ± 5.5% and 36.6% ± 2.6% of Iba1$^+$ cells were GFP negative at 0.5 and 2 weeks, respectively. Error bars indicate ± SEM. Scale bar, 10 μm.

(L–M) Time course immunohistochemical analysis of Schwann cells in nerve injury was performed on *Cx3cr1-GFP/Ccr2-RFP* rodents at 0.5, 1, 2, and 3 weeks post-injury. Representative immunohistochemical images demonstrated a sharp increase in Schwann cell numbers between 0.5 and 1 week post-injury that largely plateaued between 1 and 2 weeks (white) (L). Correlating with this, we observed a reduction in Schwann cell proliferation within the second week post-injury (10 days) compared to the first week post-injury (5 days, yellow) (N). By 2 weeks, thin myelin segments were apparent, with myelin becoming thicker by 3 weeks post-injury (red) (L). Throughout this time course, macrophages were present (green). These observations are reflected in the graphical representation (M). n = 3–4 per time point. Error bars indicate ± SEM. Scale bar, 25 μm.

(N and O) Analysis of the percentages of proliferating Schwann cells at 5 and 10 days post-injury reveals a sharp reduction in proliferating (Ki67, green) Schwann cells (Sox10, red) over time. Representative images (N) and quantification (O).

(P–S) Representative immunohistochemical images of myelin (red), macrophages (green), and Schwann cells (white) in human nerve injury. At 2 weeks post-injury, there was limited immunoreactivity for Iba1$^+$ macrophages in nerve tissue proximal to the injury site (P); instead, we found widespread phagocytic myelin-laden macrophages (Iba1$^+$ MBP$^+$) throughout the nerve distal to the injury site (Q). By 20 weeks post-injury, macrophages remained in the distal stump, although myelin debris had been cleared by this stage (R). We also observed rare instances of thin MBP$^+$ myelin segments, often in close association with p75$^+$ Schwann cells (S).

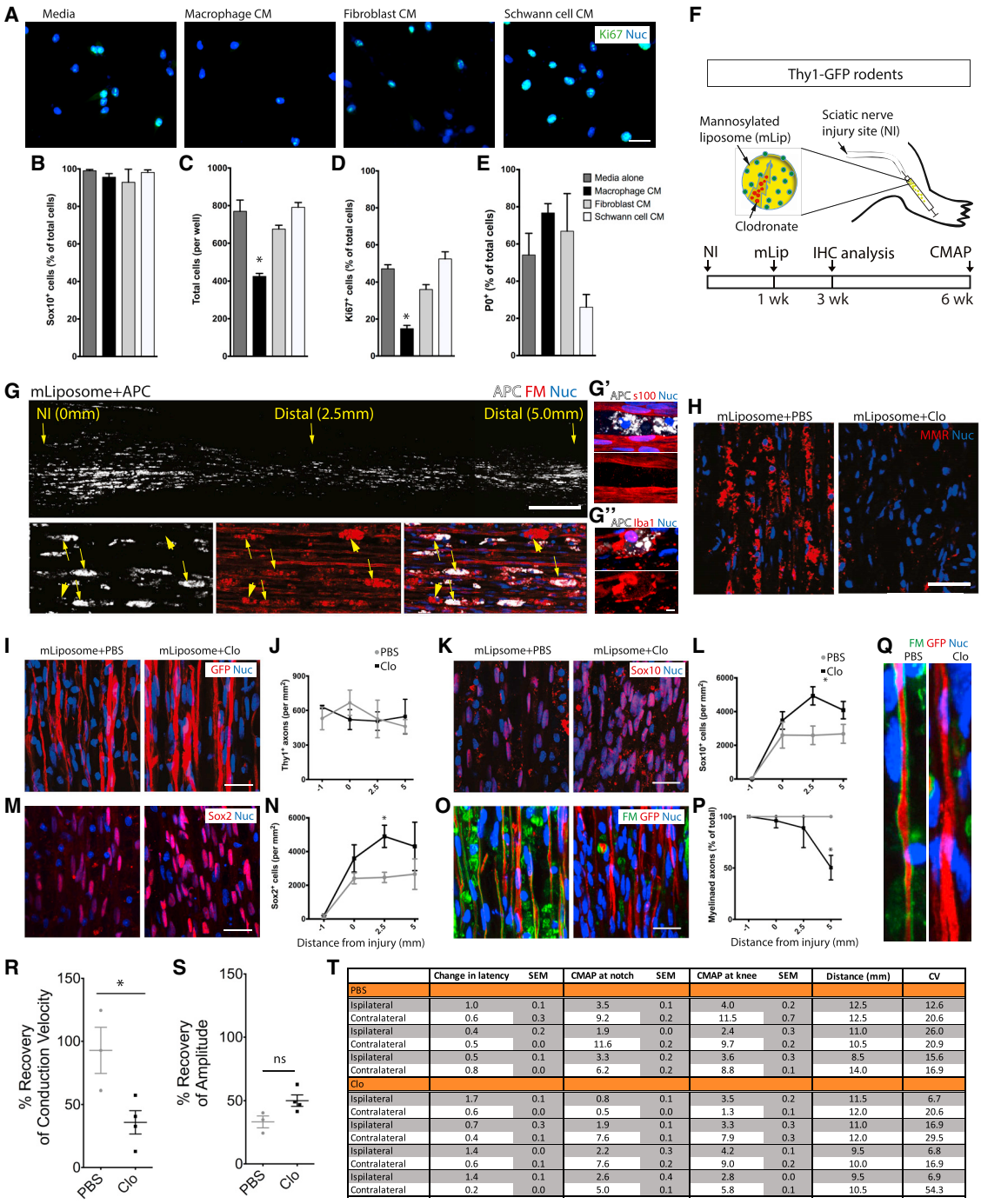

T

	Change in latency	SEM	CMAP at notch	SEM	CMAP at knee	SEM	Distance (mm)	CV
PBS								
Ispilateral	1.0	0.1	3.5	0.1	4.0	0.2	12.5	12.6
Contralateral	0.6	0.3	9.2	0.2	11.5	0.7	12.5	20.6
Ispilateral	0.4	0.2	1.9	0.0	2.4	0.3	11.0	26.0
Contralateral	0.5	0.0	11.6	0.2	9.7	0.2	10.5	20.9
Ispilateral	0.5	0.1	3.3	0.2	3.6	0.3	8.5	15.6
Contralateral	0.8	0.0	6.2	0.2	8.8	0.1	14.0	16.9
Clo								
Ispilateral	1.7	0.1	0.8	0.1	3.5	0.2	11.5	6.7
Contralateral	0.6	0.0	0.5	0.0	1.3	0.1	12.0	20.6
Ispilateral	0.7	0.3	1.9	0.1	3.3	0.3	11.0	16.9
Contralateral	0.4	0.1	7.6	0.1	7.9	0.3	12.0	29.5
Ispilateral	1.4	0.0	2.2	0.3	4.2	0.1	9.5	6.8
Contralateral	0.6	0.1	7.6	0.2	9.0	0.2	10.0	16.9
Ispilateral	1.4	0.1	2.6	0.4	2.8	0.0	9.5	6.9
Contralateral	0.2	0.0	5.0	0.1	5.8	0.1	10.5	54.3

Figure 2. Macrophages Regulate Schwann Cell Dynamics, via Secreted Factors, Instrumental for Efficient Functional Recovery following Injury

(A–E) Representative immunocytochemical images of Schwann cells coexpressing a proliferative marker, Ki67 (green), *in vitro* (A) following the addition of conditioned media (CM) from macrophages, fibroblasts, or Schwann cells. After being placed under proliferative conditions, Schwann cells that were subsequently subjected to media alone (i.e., continual proliferative stimuli) had reached ~800 cells per well, whereas Schwann cells that were subject to macrophage CM had reached ~400 cells per well (B and C) (*$p < 0.01$). Consistent with this, there was a reduction in the percentage of proliferative Schwann cells in the macrophage condition (D) (*$p < 0.01$ versus media alone). There was no difference in $P0^+$ Schwann cells in this assay (E). Error bars indicate ± SEM. Scale bar, 10 μm.

(F) Experimental design. Immunohistochemical analysis of nerve injury at 2 weeks post-injury was performed following macrophage ablation. An intraneural injection of mannosylated liposomes containing clodronate, PBS, or fluorescent proteins was made at 1 week post-injury, and then tissue was collected 1 week later.

(legend continued on next page)

Schwann cells (Figure 2G), and demonstrated that in the clodronate group, there was a 77.8% ± 3.3% reduction in (CD206) MMR-positive cells compared to vehicle controls ($p < 0.001$). Although we failed to detect any change in axonal regrowth (Figures 2I and 2J) following macrophage ablation, we found a marked effect on Schwann cells (Figures 2K–2Q). Specifically, there was an increase in the number of Schwann cells, as indicated by an increase in the number of $Sox10^+$ cells (Figures 2K and 2L) ($p < 0.01$), an increase in $Sox2^+$ immature Schwann cells (Figures 2M and 2N) ($p < 0.01$), and a significant reduction in remyelinated axons (Figures 2O–2Q) ($p < 0.001$). To examine the functional consequence, we performed compound muscle action potential (CMAP) analysis and found reduced recovery of conduction velocity (Figure 2R), but no change in amplitude (Figure 2S), by 6 weeks post-intervention ($p < 0.05$), consistent with an impairment in remyelination.

Identification of Ligands Expressed by Macrophages following Nerve Injury

To identify ligands produced by macrophages following nerve injury, we performed unbiased transcriptional profiling of macrophages 3 and 8 days after nerve injury from *Cx3cr1-GFP/Ccr2-RFP* transgenic reporter mice (Figure 3A). Monocytes from blood and macrophages from injured nerves were collected using fluorescence-activated cell sorting (FACS) and then processed for RNA sequencing (RNA-seq) analysis (Figure 3B). Only *Ccr2*-RFP and *Cx3cr1*-GFP (double positive) cells were collected for analysis, because T cells and dendritic cells express each gene, respectively, but not both (Mack et al., 2001; Sutti et al., 2015). Analysis of the top 1,000 most differentially regulated transcripts revealed a striking separation in the pattern of gene expression between monocytes and macrophages (Figure 3C). The expression of well-characterized monocyte-associated factors (*Ly6C*, *Ccr2*, and *Cx3cr1*) and macrophage-associated factors (*Aif1*, *Mrc1*, *Ccr2*, and *Cx3cr1*) was substantially different between these groups (Figures 3D–3F). We did not observe a temporal correlation of factors typically associated with a pro-inflammatory macrophage phenotype (*Il6*, *Cxcl10*, *Il12b*, *Il1b*, *Cxcl9*, and *Tnf*) or, conversely, an anti-inflammatory state (*Arg1*, *Ccl17*, *Trem2*, *Chil3*, *Stat6*, and *Retnla*) (Figures 3G and 3H). When we assessed the disease states and disorders that were represented by gene expression profiles from days 3 and 8 (Tables S1 and S2), both were most highly represented by inflammatory diseases and disorders (Ingenuity Pathway Analysis [IPA] analysis; p value: 1.8×10^{-18}–6.9×10^{-64} and 1.1×10^{-16}–5.8×10^{-53}, respectively). The top two activation *Z* scores for cellular functions under this category for day 3 were migration of phagocytes (p value: 2.8×10^{-13}) and cellular infiltration by mononuclear leukocytes (p value: 8.6×10^{-29}), and those for day 8 were migration of phagocytes (p value: 9.8×10^{-34}) and activation of phagocytes (p value: 4.3×10^{-17}). We were able to identify 529 and 1,395 genes that were uniquely expressed by day 3 and day 8 macrophages, respectively (Figure 3I; Tables S3 and S4), and of these genes, the top 3 of 5 associated bio functions were unique between the assessed time points (Figure 3J). We found that the Immune Cell Trafficking bio function was unique to day 3 and the Organismal Survival bio function was unique to day 8 (Tables S3 and S4). Consistent with a lack of concordance between time points and pro- or anti-inflammatory gene expression profiles, we found that the top 70 ligands expressed by macrophages at day 8 included both pro- and anti-inflammatory ligands (Figure 3K; Table S5).

IL-6 and Gas6 Are Expressed by Macrophages and Can Autonomously Regulate Schwann Cells *In Vitro*

From our expression data, we specifically validated three of the secreted ligands that were highly enriched in the post-injury macrophage signature (HBEGF, interleukin-6 [IL-6], and Gas6). To do this, we performed high-resolution immunofluorescence imaging and flow cytometry for HBEGF, IL-6, and Gas6 in rodent PNI, as well as *in situ* hybridization in human PNI. All three proteins were detected in the extracellular space and colocalized with what appeared to be a diverse array of cell types, including macrophages (Figures 4A–4D). Therefore, we performed intracellular flow cytometry of *Ccr2*-RFP *Cx3cr1*-GFP-positive macrophages, combined with these ligands of interest. Our analysis confirmed that all three were expressed in most *Ccr2*-RFP *Cx3cr1*-GFP-positive macrophages (HBEGF, 83.6%; IL-6, 57.5%; and Gas6, 77.2%) (Figures 4E–4H). Negative controls showed minimal immunoreactivity (Figures 4A and 4E). To determine whether similar mechanisms might contribute to endogenous repair after nerve injury in humans, we performed *in situ* hybridization for human Gas6 mRNA, combined with immunofluorescence for Iba1 in the nerve that was resected

(G) Ablation confirmation. Representative overview image of an injured nerve counterstained for myelin (red) that received fluorescent-tagged mannosylated liposomes (white, allophycocyanin [APC]). Note the spread of liposomes across the entire distal end of the nerve injury, as well as the aggregated fluorescence localized within most (arrows), but not all (arrowhead), debris-laden cells. Scale bar, 500 μm. (G′ and G″) $S100^+$ Schwann cells (red) do not colocalize with fluorescent-tagged mannosylated liposomes (G′), whereas Iba1+ macrophages (red) do (G″). Scale bar, 5 μm.

(H) Representative immunohistochemical images demonstrating a reduction in MMR-positive cells (red) following clodronate treatment (mLiposome+Clo) compared to PBS treatment (mLiposome+PBS). There was a 77.8% ± 3.3% reduction in cells immunoreactive for CD206 (*$p < 0.001$). n = 3 per time point. Error bars indicate ± SEM. Scale bar, 50 μm.

(I–Q) Targeted ablation of macrophages preceding the onset of remyelination disrupts Schwann cell dynamics. Representative immunohistochemical images demonstrating the regulation of Schwann cells (K, M, and O), but not axons (I), following clodronate treatment (mLiposome+Clo) compared to PBS treatment (mLiposome+PBS). Note the increase in $Sox10^+$ Schwann cells (red, *$p < 0.01$) (K) and $Sox2^+$ immature Schwann cell densities (red, *$p < 0.01$) (M), as well as a reduction in FM^+ myelinated axon densities (green) and Thy1-GFP^+ axon densities (red, *$p < 0.001$) (O and Q). These observations were reflected in quantification (J, L, N, and P). n = 3 per time point. Error bars indicate ± SEM. Scale bar, 25 μm.

(R–T) Targeted ablation of macrophages immediately preceding the onset of remyelination results in long-term deficits in functional recovery. Quantification of compound muscle action potential (CMAP) analysis demonstrated a reduction in recovery of conduction velocity (R) but no change in amplitude (S) at 6 weeks following clodronate treatment (Clo) compared to PBS treatment (PBS). Table of raw reads (T). n = 3–4 per time point; *$p < 0.05$. Error bars indicate ± SEM. NS, not significant; CV, conduction velocity.

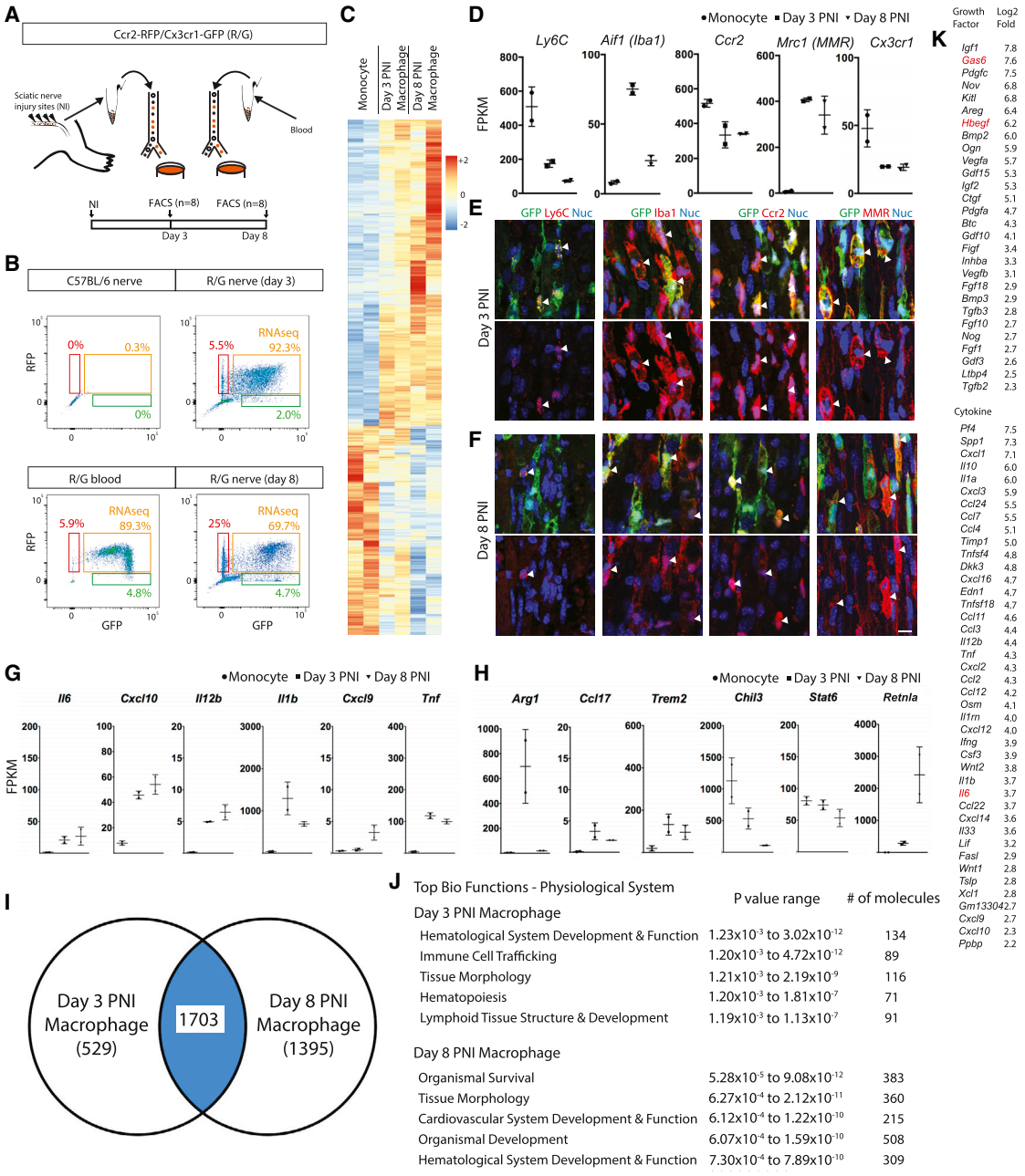

J

Top Bio Functions - Physiological System	P value range	# of molecules
Day 3 PNI Macrophage		
Hematological System Development & Function	$1.23x10^{-3}$ to $3.02x10^{-12}$	134
Immune Cell Trafficking	$1.20x10^{-3}$ to $4.72x10^{-12}$	89
Tissue Morphology	$1.21x10^{-3}$ to $2.19x10^{-9}$	116
Hematopoiesis	$1.20x10^{-3}$ to $1.81x10^{-7}$	71
Lymphoid Tissue Structure & Development	$1.19x10^{-3}$ to $1.13x10^{-7}$	91
Day 8 PNI Macrophage		
Organismal Survival	$5.28x10^{-5}$ to $9.08x10^{-12}$	383
Tissue Morphology	$6.27x10^{-4}$ to $2.12x10^{-11}$	360
Cardiovascular System Development & Function	$6.12x10^{-4}$ to $1.22x10^{-10}$	215
Organismal Development	$6.07x10^{-4}$ to $1.59x10^{-10}$	508
Hematological System Development & Function	$7.30x10^{-4}$ to $7.89x10^{-10}$	309

Figure 3. Identification of Ligands Expressed by Macrophages following Nerve Injury

(A) Experimental design. Macrophages and monocytes from *Cx3cr1-GFP/Ccr2-RFP* monocyte and macrophage reporter mice were collected using FACS at day 3 and day 8 post-sciatic nerve injury then processed for RNA-seq analysis.

(B) FACS plots depicting cell sorting of *Ccr2*-RFP and *Cx3cr1*-GFP-positive monocyte and macrophage cells from blood and injured nerve (orange boxes represent cells that were collected for RNA sequencing).

(C) Heatmap demonstrating the unique expression profile of monocytes, day 3 macrophages, and day 8 macrophages (red, fold increase; blue, fold decrease).

(D–F) Expression of well-characterized monocyte- and macrophage-associated factors. Fragments per kilobase of transcript per million mapped reads (FPKM) values (D). Representative immunohistochemical images of day 3 (E) and day 8 (F) after nerve injury, demonstrating macrophage expression of Ly6C, Aif1, *Ccr2*-RFP, Mrc1 (red), and *Cx3cr1*-GFP (green; arrowheads, colocalization) in *Cx3cr1-GFP/Ccr2-RFP* mice. Scale bar, 10 μm. Error bars indicate ± SEM.

(G and H) FPKM values of common M1 (G) and M2 (H) macrophage identifiers. Error bars indicate ± SEM.

(I) Venn diagram depicting the relationship between genetic profiles of day 3 and those of day 8 post-injury macrophages.

(J) Top bio functions in physiological systems unique to day 3 and day 8 macrophages.

(K) List of macrophage-expressed growth factors and cytokines. Factors selected for further analysis depicted in red.

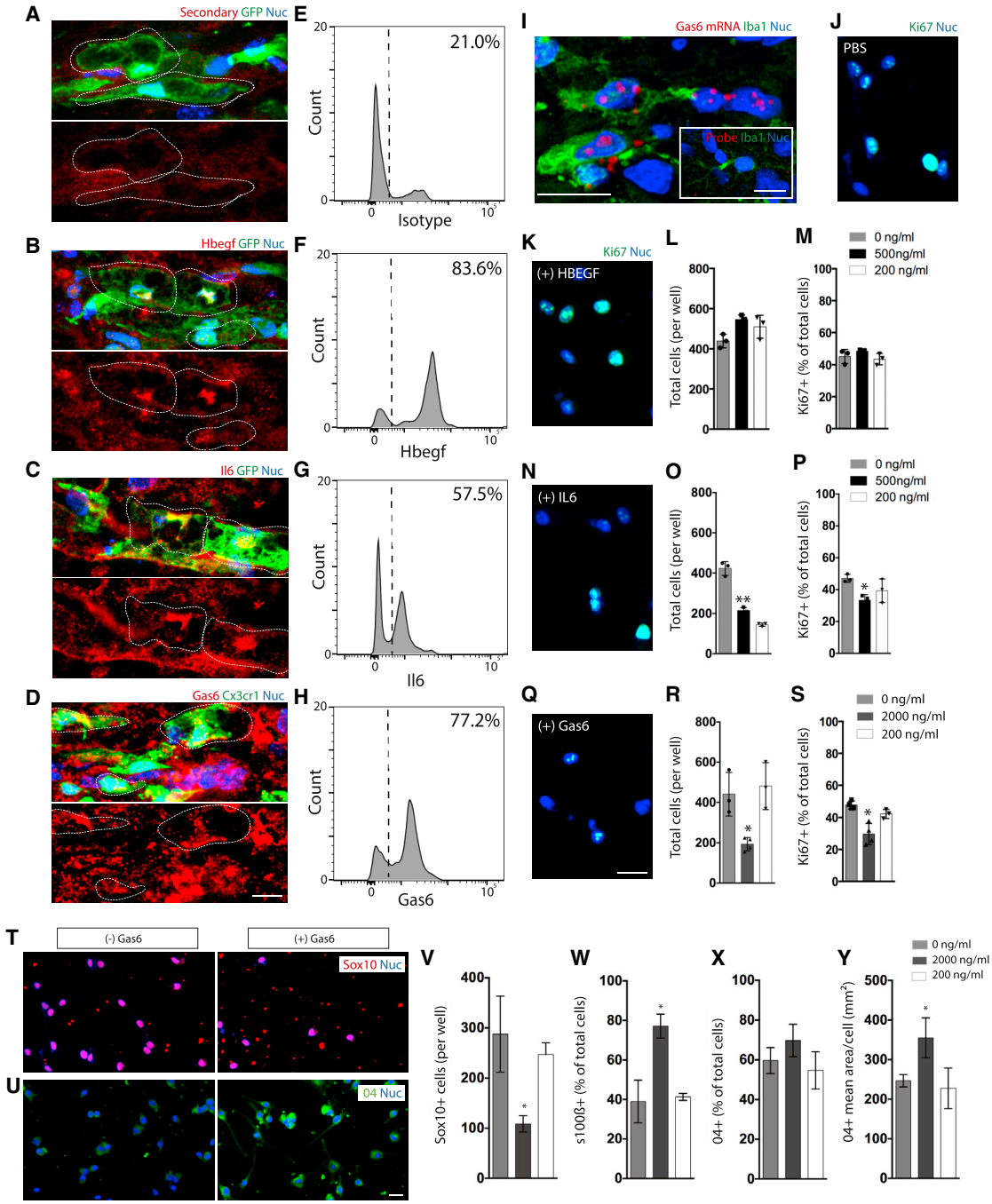

Figure 4. IL-6 and Gas6 Negatively Regulate Schwann Cell Proliferation *In Vitro*

(A–D) Representative immunohistochemical images depicting macrophages (*Cx3cr1*-GFP, green) expressing selected growth factors and cytokines (red). There was minimal evidence of immunoreactivity of macrophages in no-primary-antibody controls (A), whereas there was clear coexpression of Hbegf (B), IL-6 (C), and Gas6 (D) following the addition of these antibodies. Scale bar, 10 μm.

(E–H) Quantification of *Cx3cr1*-GFP$^+$ *Ccr2*-RFP$^+$ macrophages coexpressing selected growth factors and cytokines. No-primary-antibody controls (E), Hbegf (F), IL-6 (G), and Gas6 (H).

(I) *In situ* hybridization for Gas6 mRNA, combined with immunofluorescence staining for the macrophage marker, Iba1, in human nerve 2 weeks post-injury. Control probe (inset). Scale bar, 20 μm.

(J–S) Representative images of Schwann cells coexpressing a proliferative marker, Ki67 (green), *in vitro* following the addition of selected recombinant proteins (J, K, N, and Q). Compared to no-recombinant-protein conditions (J, M, P, and S), there was a reduction in Schwann cell proliferation and cell number in the IL-6

(legend continued on next page)

two weeks post-injury. We found that 70.9% of macrophages in the human nerve expressed Gas6 (Figure 4I). Next, we asked how exposure to either of these factors influences Schwann cell behavior *in vitro*. Adult Schwann cell cultures were grown in the presence of exogenous HBEGF, IL-6, and Gas6 and then assessed for proliferation. We found that compared to IL-6 and Gas6 conditions, media controls had a 49.2% and 56.1% increase, respectively, in total number of cells, corresponding with more (29.1% and 27.8%, respectively) mitotically active ($Ki67^+$) cells (Figures 4J–4P). Given that Gas6 is expressed by human and rodent macrophages in nerve injury, and given that it appears to have the capacity to independently regulate Schwann cell proliferation *in vitro*, we further assessed the role of Gas6 on Schwann cells *in vitro*. We found that there was more than a 2-fold increase in Schwann cells in the media control group compared to the Gas6 group (Figures 4Q and 4S) ($p < 0.01$), suggesting that the suppressed proliferation of Schwann cells by macrophages (Figures 2A–2C) at least partially depends on Gas6 activity. There was also an increase in mature Schwann cell phenotypes in the Gas6-treated group compared to untreated Schwann cells (Figures 4R and 4T–4V) ($p < 0.01$; $p < 0.05$).

Deficiency of Macrophage-Derived Gas6 Results in an Aberrant Schwann Cell Response and Compromised Remyelination

To assess the role of macrophage-derived Gas6 in nerve injury *in vivo*, we transplanted Gas6 knockout (KO) bone marrow into wild-type recipient mice (Figures 5A–5L) and examined the impact on nerve regeneration. Gas6 KO in donor mice was confirmed by PCR (Figure 5B). In parallel experiments, we confirmed the efficacy of our bone marrow transplant protocol by evaluating the percentage of transplanted *Ccr2*-RFP *Cx3cr1*-GFP-positive monocytes at two months post-irradiation and bone marrow transplant in identically irradiated recipient mice (Figures 5C and 5D). Evaluation of nerve injury in Gas6 KO recipient mice revealed an increase in Schwann cell numbers (Figures 5G and 5H) ($p < 0.006$) and a decrease in remyelinated internode length (Figures 5I–5L) ($p < 0.02$) but no difference in macrophage numbers (Figures 5E and 5F) or the total number of remyelinating myelin segments compared to control recipient mice (Figure 5K). There was also no difference in myelin thickness (average myelin thickness: control = 0.58 μm ± 0.014; Gas6 KO = 0.56 μm ± 0.017).

DISCUSSION

Although it is widely accepted that macrophages play an essential role in debris clearance and subsequent tissue remodeling after injury, understanding of how incoming or resident macrophages contribute to this process and the mechanisms by which they modulate local cell function, particularly following nerve injury, remains largely unknown. Previous studies have employed techniques to prevent monocyte infiltration or chronically ablate macrophages (Barrette et al., 2008; Chen et al., 2015; Kubota and Suzuki, 2000). For example, Barrette et al. (2008) demonstrated that loss of macrophages results in severe effects on axonal regrowth, dysregulation of neurotrophin production, and reductions in angiogenesis. However, the severity of such defects prevented meticulous analysis of processes that rely on the presence of axons, such as remyelination. Global gene KO mice have suggested that various cytokines, such as tumor necrosis factor (TNF) and interleukin-1β (IL-1β), may mediate macrophage communication during nerve regeneration (Nadeau et al., 2011), yet few macrophage-specific gene deletion experiments demonstrate definitive mechanisms by which macrophages affect nerve remodeling and regeneration. Work by Cattin et al. (2015) is one exception showing that vascular endothelial growth factor (VEGF) is a macrophage-derived factor that is essential for blood vessel formation and Schwann cell guidance following nerve injury.

Following macrophage ablation, the reductions in remyelination and conduction velocities, coupled with the increases in immature Schwann cell phenotypes, suggest that macrophages play a role in regulating Schwann cell differentiation—either by promoting remyelination or by suppressing cues to maintain an immature Schwann cell state. Schwann cells are extremely plastic, neural crest-derived glia that have several roles and phenotypes depending on the stage of development or injury state (Jessen and Mirsky, 2016). Although Schwann cells have an innate capacity to myelinate axons with minimal paracrine signaling, several extracellular factors and direct interactions with axons modulate this process (Taveggia et al., 2010). In particular, neuregulin (NRG)-1 type III, which is expressed on the axonal membrane, is a key determinant of whether Schwann cells will myelinate (Michailov et al., 2004). Other known factors that regulate myelination include non-neuronal factors such as hormones, neurotrophins, semaphorins, and laminins, yet the sources of many of these factors remain unclear (Taveggia et al., 2010). Identifying factors secreted by macrophages in nerve injury that regulate Schwann cell remyelination has largely been hindered due to a lack of accurate and unbiased genetic profiling of these cells to identify potential factors.

Several studies have used candidate approaches to describe the *in vivo* tissue-specific immune response to nerve injury (Nadeau et al., 2011; Ydens et al., 2012). Others have performed unbiased whole-tissue genetic profiling studies following nerve injury (Painter et al., 2014). By employing our macrophage- and monocyte-specific reporter system followed by FACS to prospectively isolate mobilized cells directly from injured nerve

conditions (**$p < 0.001$; *$p < 0.05$) (N–P) and Gas6 conditions (*$p < 0.01$) (Q–S). There was no difference following HBEGF treatment (K–M). Graphs indicate total $Hoechst^+$ cells and the percentage of $Ki67^+$ $Hoechst^+$ double-positive cells. Error bars indicate ± SEM. Scale bar, 10 μm.

(T–Y) Application of recombinant Gas6 protein to Schwann cell cultures resulted in a reduction in total Schwann cell numbers (T and V) and an increase in mature Schwann cell phenotypes (U and W–Y). Representative immunocytochemical images of cultures immunoreactive for a pan-Schwann cell marker, Sox10 (red) (T), and a mature Schwann cell marker, O4 (green) (U). (V–Y) Quantification revealed a significant reduction in Schwann cell numbers (*$p < 0.01$ versus 0 ng/mL) (V), as well as an increase in the percentage of mature $s100b^+$ Schwann cells (*$p < 0.01$ versus 0 ng/mL) (W) and an increase in the area of $O4^+$ Schwann cells (*$p < 0.05$ versus 0 ng/mL) (Y). n = 3 per condition. Error bars indicate ± SEM. Scale bar, 10 μm.

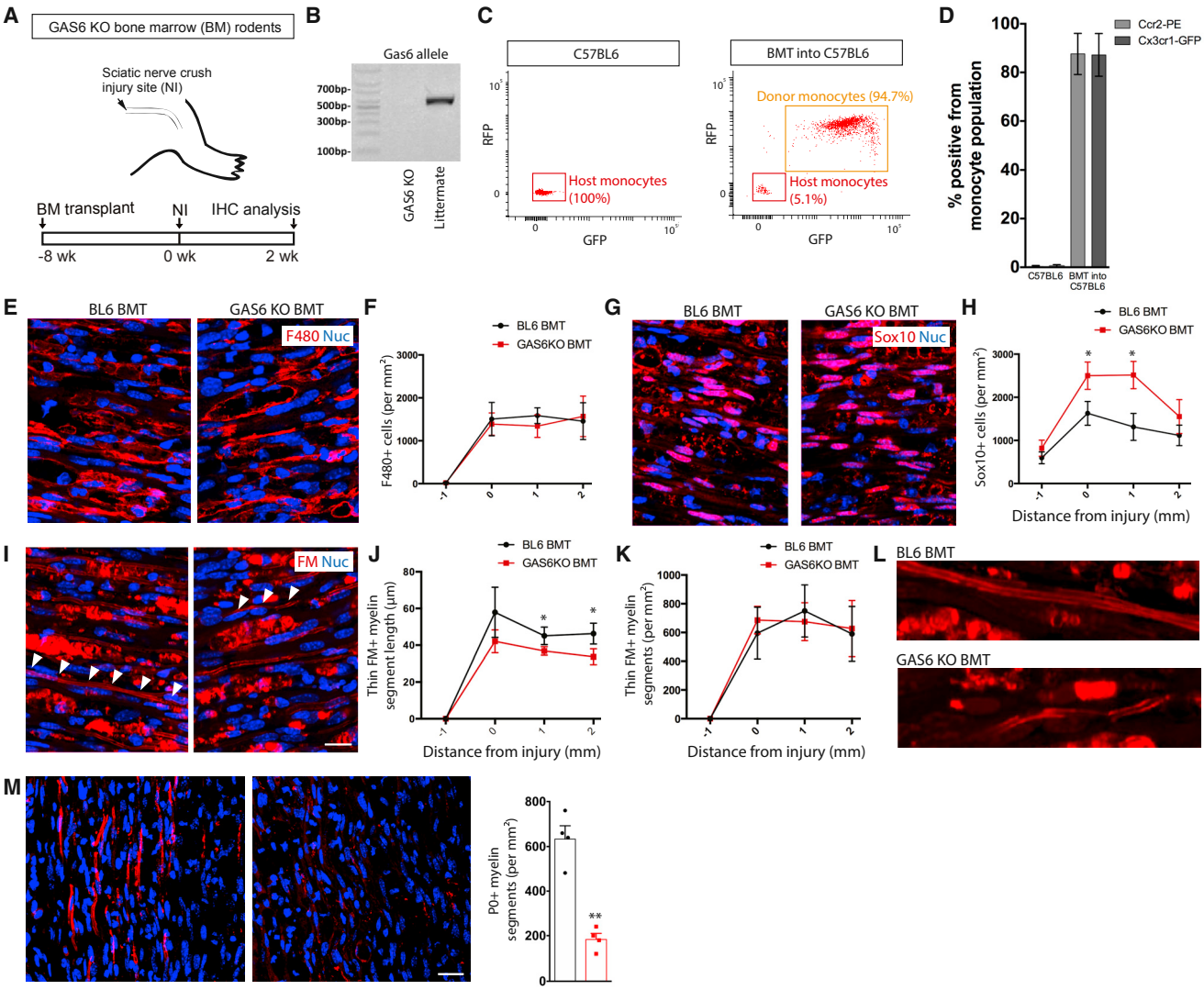

Figure 5. Gas6 Regulates Schwann Cell Maturation *In Vivo*

(A) Experimental design for (B)–(L). Immunohistochemical analysis of nerve injury at 2 weeks post-injury was performed in rodents that underwent Gas6 knockout (KO) bone marrow transplants. Two months before injury, *C57BL/6* recipient rodents were irradiated and then received a tail vein injection of 400,000 Gas6 KO or *C57BL/6* bone marrow cells.

(B–D) KO confirmation. PCR for Gas6 wild-type allele confirming that expected band at 530 bp was absence in KO mice (using genomic tail DNA) (B). Bone marrow transplant was confirmed by assessing the percentage of *Ccr2*-RFP$^+$ and *Cx3cr1*-GFP$^+$ monocytes at two months post-irradiation and bone marrow transplant in irradiated recipient mice that had received cells from macrophage reporter mice (*Cx3cr1-GFP/Ccr2-RFP*) (C and D).

(E–M) Macrophage-targeted Gas6 KO *in vivo* increased Schwann cell numbers (*$p < 0.006$) (G and H) and caused a decrease in remyelinated internode length (*$p < 0.02$) (I and J) and a decrease in P0+ myelin segments (**$p < 0.001$) (M). Representative immunohistochemical images and quantification of cells immunoreactive for a pan-macrophage marker, F480 (E and F), and a pan-Schwann cell marker, Sox10 (*$p < 0.006$) (G and H), as well as a myelin lipid marker, Fluoromyelin (FM) (I–L), and myelin protein (P0) (red) (M). n = 5 per time point. Error bars indicate ± SEM. Scale bar, 25 μm.

and blood, it enables us to more readily identify macrophage genes of interest in an unbiased fashion *in vivo*. In contrast to Painter et al. (2014), who used whole-tissue microarrays at a similar time point, we found that *Retnla* and *Gas6* were two of the most highly expressed macrophage-associated genes (these same genes were downregulated in their dataset). *Pdgfc*, *Areg*, *Il1a*, *Cxcl3*, *Vegfa*, *Il10*, *Gdf15*, *IL6*, *Cxcl10*, and *Il1rn* were unchanged in the Painter et al. (2014) dataset set yet were upregulated in our dataset. Our data identify several candidate immunomodulatory factors within the injured peripheral nerve and highlight the importance of including population-specific gene expression studies, particularly undifferentiated population controls, to better elucidate cell-type-specific transcriptional changes within injured tissues (Shah et al., 2018).

We were surprised to find that genes associated with either classic inflammatory macrophage (M1) or anti-inflammatory macrophage (M2) phenotypes *in vitro* did not correlate with either time point (3 or 8 days post-injury) analyzed within our

in vivo dataset (Jablonski et al., 2016). There is a suggestion that macrophages, in most tissues, transition from a pro-inflammatory to a pro-regenerative and anti-inflammatory macrophage over time (Arnold et al., 2007; Dal-Secco et al., 2015), yet the transcriptional profile of nerve injury-derived macrophages, assessed over time, demonstrates that injury stage had a relatively minor influence on the overall pattern of gene expression, at least for most classic pro- or anti-inflammatory genes. For example, the M2 genes *Arg1* and *Chil3* were present at day 3 yet were barely expressed at day 8, and the M1 and M2 genes *Il6*, *Cxcl10*, *Il12b*, *Trem2*, and *Tnf* were expressed at similar levels at both day 3 and day 8 post-injury. This was also the case for secreted factors: *Igf1* was one of the only secreted factors upregulated in day 8 macrophages compared to day 3 macrophages. Instead, changes over time were gene signatures involved in cellular infiltration and trafficking (for day 3) and activation of phagocytes (for day 8), which is consistent with monocytes still actively infiltrating the injury site at day 3 and macrophages actively phagocytizing debris at day 8. It would be interesting to assess macrophages at day 1 post-injury to ascertain whether this acute time point is more representative of a classic M1. Nevertheless, given the lack of major differences across time, it is likely that the described transcriptional profile identified here at both day 3 and day 8 largely captures a representative *in vivo* nerve injury-induced macrophage gene signature. Now that we have defined a macrophage gene signature in healthy acute injury, future experiments endeavor to compare this signature to the macrophage gene signature in compromised or chronically denervated nerve injury environments with the hopes of identifying dysregulated pathways that can be therapeutically modulated.

We identified several macrophage-derived factors that have previously been shown to regulate Schwann cell maturation (Haggiag et al., 1999; Wakatsuki et al., 2009; Miyamoto et al., 2015), validating our results. Gas6 had not been explored in nerve injury, and we found that it was highly enriched in post-injury macrophages and, when genetically deleted from the hematopoietic lineage, resulted in impaired remyelination. We also observed that Gas6 mRNA was specifically expressed in macrophage within the adult injured human nerve, suggesting that Gas6 may be a viable pharmacological target to modulate Schwann cell function to hasten or improve axonal remyelination in humans. Schwann cells express the TAM tyrosine kinase receptor, TYRO3, a receptor that binds Gas6 with high affinity. TYRO3 can act via Fyn tyrosine kinase and Akt to support developmental myelination but does not appear to be involved in the regulation of Schwann cell proliferation or cell death, at least during development in rodents (Miyamoto et al., 2015). In human Schwann cells *in vitro*, Gas6 may function via the regulation of extracellular signal-regulated kinase (ERK-2) to promote proliferation (Li et al., 1996), contrasting our *in vitro* results in mouse at higher doses. However, the role that Gas6 plays in PNS injury *in vivo* is unknown. In the CNS, using a model of demyelination in the corpus callosum, it was reported that Gas6 enhanced remyelination and prevented demyelination (Tsiperson et al., 2010). Given that we have observed an increase in Schwann cell numbers and defects in remyelination following macrophage-targeted Gas6 KO, it is possible that during regeneration in the injured nerve, macrophage-derived Gas6 plays a direct role in regulating several processes, including remyelination, cell survival, and cell proliferation via multiple pathways (Angelillo-Scherrer et al., 2008). It is also possible that macrophage-derived Gas6 regulates processes in other cell types, including proliferation and cell migration of vascular smooth muscle cells (Nakano et al., 1997) and survival of endothelial cells (D'Arcangelo et al., 2002), which we have not assessed. Finally, as per our dataset, given that macrophages in nerve injury express *Axl* and *Mertk* (other Gas6 receptors), it is likely that Gas6 plays an autocrine role in macrophages. Others have shown subtle alterations in cytokine secretion in Gas6 KO macrophages that could indirectly regulate Schwann cells and could regulate macrophage phagocytic capacity (Angelillo-Scherrer et al., 2008).

STAR★METHODS

Detailed methods are provided in the online version of this paper and include the following:

- KEY RESOURCES TABLE
- CONTACT FOR REAGENT AND RESOURCE SHARING
- EXPERIMENTAL MODEL AND SUBJECT DETAILS
  - Animals
- METHOD DETAILS
  - Bone marrow transplants
  - Rodent nerve injuries
  - Macrophage ablation and CMAPs
  - Immunohistochemistry and *in situ* hybridization
  - *In vitro* Schwann cell experiments
  - Macrophage FACs isolations & RNaseq
  - RNaseq bioinformatics
  - Flow cytometry to detect intracellular cytokines
- QUANTIFICATION AND STATISTICAL ANALYSIS
- DATA AND SOFTWARE AVAILABILITY

SUPPLEMENTAL INFORMATION

Supplemental Information includes five tables and can be found with this article online at https://doi.org/10.1016/j.celrep.2018.08.004.

ACKNOWLEDGMENTS

We acknowledge the support provided by technical staff, including Dr, Min Cheng, Jessica SuMee Yoon, and Anowara Islam. Special thanks to Dr. Bridget Shafit-Zagardo and Dr. Juwen C. DuBois at the Albert Einstein College of Medicine for gifting us Gas6 KO bones. We also thank the staff at the Regeneration Unit in Neurobiology (RUN) facility, UCDNA Services Facility, as well as the Animal Care facility staff at the University of Calgary. This work was funded by an Alberta Innovates Health Solutions (AIHS) grant (201200859 to R.M. and J.B.), a CIHR New Investigator Award (J.B.), an Alberta Children's Health Research Institute Fellowship (J.A.S.), an Alberta Innovates Health Solutions Scholarship and a BSc Neuroscience Undergraduate Research Scholarship (both to A.H.), a CIHR grant (T.T.), and AIHS and CIHR doctorate scholarships (N.E.B.).

AUTHOR CONTRIBUTIONS

J.A.S., R.M., and J.B. designed the experiments. J.A.S., A.H., S.S., N.E.B., N.L.R., and M.V. performed the experiments and analyzed the data. J.A.S.

and J.B. wrote the paper. R.M., T.T., A.H., S.S., N.E.B., N.L.R., and M.V. read and edited the paper.

DECLARATION OF INTERESTS

The authors declare no competing interests.

Received: November 22, 2017
Revised: April 15, 2018
Accepted: July 29, 2018
Published: September 4, 2018

REFERENCES

Angelillo-Scherrer, A., de Frutos, P., Aparicio, C., Melis, E., Savi, P., Lupu, F., Arnout, J., Dewerchin, M., Hoylaerts, M., Herbert, J., et al. (2001). Deficiency or inhibition of Gas6 causes platelet dysfunction and protects mice against thrombosis. Nat. Med. *7*, 215–221.

Angelillo-Scherrer, A., Burnier, L., Lambrechts, D., Fish, R.J., Tjwa, M., Plaisance, S., Sugamele, R., DeMol, M., Martinez-Soria, E., Maxwell, P.H., et al. (2008). Role of Gas6 in erythropoiesis and anemia in mice. J. Clin. Invest. *118*, 583–596.

Arnold, L., Henry, A., Poron, F., Baba-Amer, Y., van Rooijen, N., Plonquet, A., Gherardi, R.K., and Chazaud, B. (2007). Inflammatory monocytes recruited after skeletal muscle injury switch into antiinflammatory macrophages to support myogenesis. J. Exp. Med. *204*, 1057–1069.

Barrette, B., Hébert, M.A., Filali, M., Lafortune, K., Vallières, N., Gowing, G., Julien, J.P., and Lacroix, S. (2008). Requirement of myeloid cells for axon regeneration. J. Neurosci. *28*, 9363–9376.

Biernaskie, J., Paris, M., Morozova, O., Fagan, B.M., Marra, M., Pevny, L., and Miller, F.D. (2009). SKPs derive from hair follicle precursors and exhibit properties of adult dermal stem cells. Cell Stem Cell *5*, 610–623.

Cattin, A.L., Burden, J.J., Van Emmenis, L., Mackenzie, F.E., Hoving, J.J., Garcia Calavia, N., Guo, Y., McLaughlin, M., Rosenberg, L.H., Quereda, V., et al. (2015). Macrophage-induced blood vessels guide Schwann cell-mediated regeneration of peripheral nerves. Cell *162*, 1127–1139.

Chen, P., Piao, X., and Bonaldo, P. (2015). Role of macrophages in Wallerian degeneration and axonal regeneration after peripheral nerve injury. Acta Neuropathol. *130*, 605–618.

D'Arcangelo, D., Gaetano, C., and Capogrossi, M.C. (2002). Acidification prevents endothelial cell apoptosis by Axl activation. Circ. Res. *91*, e4–e12.

Dal-Secco, D., Wang, J., Zeng, Z., Kolaczkowska, E., Wong, C.H., Petri, B., Ransohoff, R.M., Charo, I.F., Jenne, C.N., and Kubes, P. (2015). A dynamic spectrum of monocytes arising from the *in situ* reprogramming of CCR2+ monocytes at a site of sterile injury. J. Exp. Med. *212*, 447–456.

Gordon, S., and Plüddemann, A. (2017). Tissue macrophages: heterogeneity and functions. BMC Biol. *15*, 53.

Gruber, R.C., Ray, A.K., Johndrow, C.T., Guzik, H., Burek, D., de Frutos, P.G., and Shafit-Zagardo, B. (2014). Targeted GAS6 delivery to the CNS protects axons from damage during experimental autoimmune encephalomyelitis. J. Neurosci. *34*, 16320–16335.

Haggiag, S., Chebath, J., and Revel, M. (1999). Induction of myelin gene expression in Schwann cell cultures by an interleukin-6 receptor-interleukin-6 chimera. FEBS Lett. *457*, 200–204.

Jablonski, K.A., Gaudet, A.D., Amici, S.A., Popovich, P.G., and Guerau-de-Arellano, M. (2016). Control of the inflammatory macrophage transcriptional signature by miR-155. PLoS ONE *11*, e0159724.

Jessen, K.R., and Mirsky, R. (2016). The repair Schwann cell and its function in regenerating nerves. J. Physiol. *594*, 3521–3531.

Jung, T., Schauer, U., Heusser, C., Neumann, C., and Rieger, C. (1993). Detection of intracellular cytokines by flow cytometry. J. Immunol. Methods *159*, 197–207.

Kubota, A., and Suzuki, K. (2000). Effect of liposome-mediated macrophage depletion on Schwann cell proliferation during Wallerian degeneration. J. Neurotrauma *17*, 789–798.

Lawrence, M., Huber, W., Pagès, H., Aboyoun, P., Carlson, M., Gentleman, R., Morgan, M.T., and Carey, V.J. (2013). Software for computing and annotating genomic ranges. PLoS Comput. Biol. *9*, e1003118.

Li, R., Chen, J., Hammonds, G., Phillips, H., Armanini, M., Wood, P., Bunge, R., Godowski, P.J., Sliwkowski, M.X., and Mather, J.P. (1996). Identification of Gas6 as a growth factor for human Schwann cells. J. Neurosci. *16*, 2012–2019.

Lim, E.F., Nakanishi, S.T., Hoghooghi, V., Eaton, S.E., Palmer, A.L., Frederick, A., Stratton, J.A., Stykel, M.G., Whelan, P.J., Zochodne, D.W., et al. (2017). AlphaB-crystallin regulates remyelination after peripheral nerve injury. Proc. Natl. Acad. Sci. USA *114*, E1707–E1716.

Love, M.I., Huber, W., and Anders, S. (2014). Moderated estimation of fold change and dispersion for RNA-seq data with DESeq2. Genome Biol. *15*, 550.

Mack, M., Cihak, J., Simonis, C., Luckow, B., Proudfoot, A.E., Plachý, J., Brühl, H., Frink, M., Anders, H.J., Vielhauer, V., et al. (2001). Expression and characterization of the chemokine receptors CCR2 and CCR5 in mice. J. Immunol. *166*, 4697–4704.

Martini, R., Fischer, S., López-Vales, R., and David, S. (2008). Interactions between Schwann cells and macrophages in injury and inherited demyelinating disease. Glia *56*, 1566–1577.

Michailov, G.V., Sereda, M.W., Brinkmann, B.G., Fischer, T.M., Haug, B., Birchmeier, C., Role, L., Lai, C., Schwab, M.H., and Nave, K.A. (2004). Axonal neuregulin-1 regulates myelin sheath thickness. Science *304*, 700–703.

Mirfeizi, L., Stratton, J.A., Kumar, R., Shah, P., Agabalyan, N., Stykel, M.G., Midha, R., Biernaskie, J., and Kallos, M.S. (2017). Serum-free bioprocessing of adult human and rodent skin-derived Schwann cells: implications for cell therapy in nervous system injury. J. Tissue Eng. Regen. Med. *11*, 3385–3397.

Miron, V.E., Boyd, A., Zhao, J.-W., Yuen, T.J., Ruckh, J.M., Shadrach, J.L., van Wijngaarden, P., Wagers, A.J., Williams, A., Franklin, R.J.M., and Ffrench-Constant, C. (2013). M2 microglia and macrophages drive oligodendrocyte differentiation during CNS remyelination. Nat. Neurosci. *16*, 1211–1218.

Miyamoto, Y., Torii, T., Takada, S., Ohno, N., Saitoh, Y., Nakamura, K., Ito, A., Ogata, T., Terada, N., Tanoue, A., and Yamauchi, J. (2015). Involvement of the Tyro3 receptor and its intracellular partner Fyn signaling in Schwann cell myelination. Mol. Biol. Cell *26*, 3489–3503.

Moore, A.M., Borschel, G.H., Santosa, K.A., Flagg, E.R., Tong, A.Y., Kasukurthi, R., Newton, P., Yan, Y., Hunter, D.A., Johnson, P.J., and Mackinnon, S.E. (2012). A transgenic rat expressing green fluorescent protein (GFP) in peripheral nerves provides a new hindlimb model for the study of nerve injury and regeneration. J. Neurosci. Methods *204*, 19–27.

Nadeau, S., Filali, M., Zhang, J., Kerr, B.J., Rivest, S., Soulet, D., Iwakura, Y., de Rivero Vaccari, J.P., Keane, R.W., and Lacroix, S. (2011). Functional recovery after peripheral nerve injury is dependent on the pro-inflammatory cytokines IL-1β and TNF: implications for neuropathic pain. J. Neurosci. *31*, 12533–12542.

Nakano, T., Kawamoto, K., Kishino, J., Nomura, K., Higashino, K., and Arita, H. (1997). Requirement of gamma-carboxyglutamic acid residues for the biological activity of Gas6: contribution of endogenous Gas6 to the proliferation of vascular smooth muscle cells. Biochem. J. *323*, 387–392.

Noble, J., Munro, C.A., Prasad, V.S., and Midha, R. (1998). Analysis of upper and lower extremity peripheral nerve injuries in a population of patients with multiple injuries. J. Trauma *45*, 116–122.

Oluich, L.-J., Stratton, J.A.S., Xing, Y.L., Ng, S.W., Cate, H.S., Sah, P., Windels, F., Kilpatrick, T.J., and Merson, T.D. (2012). Targeted ablation of oligodendrocytes induces axonal pathology independent of overt demyelination. J. Neurosci. *32*, 8317–8330.

Painter, M.W., Brosius Lutz, A., Cheng, Y.C., Latremoliere, A., Duong, K., Miller, C.M., Posada, S., Cobos, E.J., Zhang, A.X., Wagers, A.J., et al. (2014). Diminished Schwann cell repair responses underlie age-associated impaired axonal regeneration. Neuron *83*, 331–343.

Shah, P.T., Stratton, J.A., Stykel, M.G., Abbasi, S., Sharma, S., Mayr, K.A., Koblinger, K., Whelan, P.J., and Biernaskie, J. (2018). Single-cell transcriptomics and fate mapping of ependymal cells reveals an absence of neural stem cell function. Cell *173*, 1045–1057.

Siemionow, M., and Brzezicki, G. (2009). Chapter 8: current techniques and concepts in peripheral nerve repair. Int. Rev. Neurobiol. *87*, 141–172.

Stratton, J.A., and Shah, P.T. (2016). Macrophage polarization in nerve injury: do Schwann cells play a role? Neural Regen. Res. *11*, 53–57.

Stratton, J.A., Shah, P.T., Kumar, R., Stykel, M.G., Shapira, Y., Grochmal, J., Guo, G.F., Biernaskie, J., and Midha, R. (2016). The immunomodulatory properties of adult skin-derived precursor Schwann cells: implications for peripheral nerve injury therapy. Eur. J. Neurosci. *43*, 365–375.

Stratton, J.A., Kumar, R., Sinha, S., Shah, P., Stykel, M., Shapira, Y., Midha, R., and Biernaskie, J. (2017). Purification and characterization of Schwann cells from adult human skin and nerve. eNeuro *4*, 1–16.

Sutti, S., Locatelli, I., Bruzzì, S., Jindal, A., Vacchiano, M., Bozzola, C., and Albano, E. (2015). CX3CR1-expressing inflammatory dendritic cells contribute to the progression of steatohepatitis. Clin. Sci. (Lond.) *129*, 797–808.

Taveggia, C., Feltri, M.L., and Wrabetz, L. (2010). Signals to promote myelin formation and repair. Nat. Rev. Neurol. *6*, 276–287.

Tsiperson, V., Li, X., Schwartz, G.J., Raine, C.S., and Shafit-Zagardo, B. (2010). GAS6 enhances repair following cuprizone-induced demyelination. PLoS ONE *5*, e15748.

Wakatsuki, S., Yumoto, N., Komatsu, K., Araki, T., and Sehara-Fujisawa, A. (2009). Roles of meltrin-beta/ADAM19 in progression of Schwann cell differentiation and myelination during sciatic nerve regeneration. J. Biol. Chem. *284*, 2957–2966.

Wang, X., Chen, H., Tian, R., Zhang, Y., Drutskaya, M.S., Wang, C., Ge, J., Fan, Z., Kong, D., Wang, X., et al. (2017). Macrophages induce AKT/β-catenin-dependent Lgr5^{+} stem cell activation and hair follicle regeneration through TNF. Nat. Commun. *8*, 14091.

Ydens, E., Cauwels, A., Asselbergh, B., Goethals, S., Peeraer, L., Lornet, G., Almeida-Souza, L., Van Ginderachter, J.A., Timmerman, V., and Janssens, S. (2012). Acute injury in the peripheral nervous system triggers an alternative macrophage response. J. Neuroinflammation *9*, 176.

STAR★METHODS

KEY RESOURCES TABLE

REAGENT or RESOURCE	SOURCE	IDENTIFIER
Antibodies		
anti-Iba1 (rabbit, 1:200)	Wako	Cat#019-19741; RRID: AB_839504
anti-Cx3cr1 (rabbit, 1:500)	Torrey Pines Biolabs Inc	Cat#TP501; RRID: AB_10892355
anti-CD68 (mouse, 1:200)	Biorad	Cat#MCA341R; RRID: AB_2291300
anti-Ly6C (APC-conjugated, 1:50)	BD Biosciences	Cat#AL-21; RRID: AB_1727554
anti-CD206 (goat, 1:200),	R&D	Cat#AF2535; RRID: AB_2063012
anti-P0 (chicken, 1:200)	Aves lab	Cat#PZ0; RRID: 427811
anti-Ki67 (rat, 1:200)	ThermoFisher	Cat#14-5698-82; RRID: AB_10854564
anti-Sox2 (goat, 1:200)	Santa Cruz	Cat#sc-17320; RRID: AB_2286684
anti-Sox10 (goat, 1:200)	Santa Cruz	Cat#sc-17343; RRID: AB_2255319
anti-HBEGF (goat, 1:100)	R&D	Cat#AF259NA; RRID: AB_354429
anti-Gas6 (rabbit, 1:100)	Santa Cruz	Cat#sc22759; RRID: AB_2108071
anti-p75 (rabbit, 1:200)	Promega	Cat#G323A; RRID: AB_430853
anti-S100β (rabbit, 1:200)	Dako	Cat#Z0311; RRID: AB_10013383
anti-O4 (FITC-conjugated, 1:50)	Millipore	Cat#MAB345A4; RRID: AB_11204899
anti-s100 (rabbit, 1:500)	Dako	Cat#Z0311; RRID: AB_10013383
anti-Thy1 (mouse, 1:500)	Covance	Cat#MMS-435P; RRID: AB_2313773
anti-IL6 (goat, 1:100)	R&D	Cat#af506; RRID: AB_355398
Biological Samples		
Human nerve injury FFPE slides	Foothills Hospital, University of Calgary, Calgary, Alberta, Canada	Alberta Provincial Research Ethics Board (REB16-1503)
Chemicals, Peptides, and Recombinant Proteins		
Mannosylated Liposomes	Clodrosome	Cat#8907RRID#AB_2687696
HBEGF	Peprotec	Cat#100-47
Gas6	R&D	Cat#CF 885-GSB-050
IL-6	R&D	Cat#506-RL-010
Critical Commercial Assays		
RNA extraction kit	Ambion	Cat#AM1561
Reverse transcription and Multiple Displacement Amplification with REPLI-g SensiPhi DNA Polymerase and oligo-dT primers	QIAGEN	Cat#150073
Library prep using GeneRead Adaptor I Set A 12-plex index adapters	QIAGEN	Cat#180985
High-output v2 75 cycle sequencing kit (for NextSeq 500 sequencer)	Illumina	Cat#FC-404-2005
Gas6 (human) in situ probes	Advanced Cell Diagnostics	Cat#427811
Deposited Data		
High throughput sequencing	This paper	GEO: GSE106927
Experimental Models: Cell Lines		
Adult mouse Schwann cells	This paper	N/A
Experimental Models: Organisms/Strains		
Rats: SD-Tg(CAG-EGFP)$^{+/-}$	The National BioResource Project for the Rat in Japan	NBRP#0235
Mice: Cx3cr1-GFP$^{+/-}$: Ccr2-RFP$^{+/-}$	Jackson Laboratories	#017586; #005582
Rats: Thy1-GFP$^{+/-}$	Moore et al., 2012	N/A

(*Continued on next page*)

Continued

REAGENT or RESOURCE	SOURCE	IDENTIFIER
Mice: Gas6$^{-/-}$	Angelillo-Scherrer et al., 2001; Gruber et al., 2014	N/A
Oligonucleotides		
Gas6 targeting sequence (mouse): 5′-AGCTGCTCGAG GCGCTGTTGCCGGCGC-3′ and 5′-AGCTGCTCGAGG ACCAGTGCACGCCCAACC-3′	Angelillo-Scherrer et al., 2001	N/A
Software and Algorithms		
Bcl to Fastq conversion	bcl2fastq software	https://www.illumina.com/
Alignment against mm10 reference genome	bwa 0.7.12 in "mem" alignment mode	Lawrence et al., 2013
GenomicAlignments, Pheatmap, and DESeq2	N/A	Love et al., 2014

CONTACT FOR REAGENT AND RESOURCE SHARING

Further information and requests for resources and reagents should be directed to and will be fulfilled by the Lead Contact, Jeff Biernaskie (jeff.biernaskie@ucalgary.ca).

EXPERIMENTAL MODEL AND SUBJECT DETAILS

Animal work was carried out in accordance with the guidelines and regulations of the CCAC and received prior approval from the University of Calgary's Animal Care Committee (protocol AC14-0019). Permission to acquire archived human traumatic nerve tissue for evaluation was approved by the University of Calgary as well as the Alberta Provincial Research Ethics Board (REB16-1503).

Animals

GFP rats

Rats were maintained at the University of Calgary's Animal Facility, under standard rat housing conditions. This included housing in pairs under a 12-hour light-dark cycle, at 20-24°C, with unlimited food and water. GFP rats (SLC, Japan) were on a Sprague-Dawley background (Biernaskie et al., 2009) and were maintained via crossing GFP$^{+/-}$ and GFP$^{-/-}$ rats to obtain GFP$^{+/-}$ and GFP$^{-/-}$ offspring for experimentation. GFP$^{-/-}$ female rats were randomly assigned to each group, while male GFP$^{+/-}$ littermates were used as bone marrow donors. Rats were maintained in sterile conditions in the Animal Facility for two months before nerve injury, then another 0-2 weeks after nerve injury. A total of 12 female rats were used for an immunohistochemical nerve injury time course experiment (n = 4 per time point at day 0, 3 and 14 days post-nerve injury).

Cx3cr1-GFP/Ccr2-RFP mice

Mice were maintained at the University of Calgary's Animal Facility, under standard housing conditions. This included housing with 4-5 mice under a 12-hour light-dark cycle, at 20-24°C, with unlimited food and water. *Cx3cr1-GFP/Ccr2-RFP* mice on a *C57BL/6* background (stock no.: 017586; stock No.: 005582, Jackson Laboratories), were kindly donated by Dr. Kubes (University of Calgary) in 2014. Mice were maintained via crossing *Cx3cr1-GFP*$^{+/+}$ Ccr2-*RFP*$^{+/+}$ male and *C57BL/6* female mice to obtain *Cx3cr1-GFP*$^{+/-}$ *Ccr2-RFP*$^{+/-}$ heterozygous offspring where both monocytes and macrophages were confirmed to have GFP and RFP reporters (Dal-Secco et al., 2015). Female mice (weights: ~30 g) at postnatal day 60 to 90 were randomly assigned to each group as defined below.

Five experiments were performed using these macrophage reporter mice. 1) An immunohistochemical nerve injury time-course experiment including 0, 3, 7, 14 and 21 days post nerve injury (n = 4 per time point). 2) RNaseq experiment, as outlined below, using n = 7-8 mice per time point at Day 3 and 8 post-nerve injury. 3) Validation of RNaseq experiment using flow cytometry, as outlined below, using n = 3 mice at 8 days post-nerve injury. 4) CMAP analysis, as outlined below, using n = 7 mice at 8 weeks post-nerve injury. 5) Validation of bone marrow transplant take. Bone marrow from 5 *Cx3cr1-GFP/Ccr2-RFP* reporter mice were transplanted into five *C57BL/6* wild-type mice and processed in the same fashion as Gas6 KO experiments, but instead of immunohistochemical analysis, the percentage of *Cx3cr1*-GFP *Ccr2*-RFP positive monocytes was assessed at 8 weeks post bone marrow transplant.

Thy1-GFP rats

Rats were maintained at the University of Calgary's Animal Facility, under standard housing conditions. This included housing in pairs under a 12-hour light-dark cycle, at 20-24°C, with unlimited food and water. *Thy1-GFP*$^{+/-}$ rats on a Sprague-Dawley background (Moore et al., 2012) (herein referred to as *Thy1-GFP* rats) were kindly donated by Dr. Borschel. Rats were maintained by crossing *Thy1-GFP*$^{+/-}$ male and *Thy1-GFP*$^{+/-}$ female rats to obtain *Thy1-GFP* heterozygote offspring for experimentation. Female rats (~150 g) at postnatal day 90 were used. A total of 9 female rats were randomly assigned to each group to assess the effects

of macrophage ablation on Schwann cell dynamics. Experimental groups included: mannosylated liposomes encapsulating either clodronate (n = 3), PBS (n = 3) or APC (n = 3).

Gas6 KO mice

Mice were maintained at the University of Calgary's Animal Facility, under standard housing conditions. This included housing with 4-5 mice under a 12-hour light-dark cycle, at 20-24°C, with unlimited food and water. Femur bones from 7-week old male *Gas6*$^{-/-}$ mice (n = 6 bones) backcrossed onto a *C57BL/6* background (Jackson Laboratory) (herein referred to as *Gas6* KO) were kindly provided by Dr Shafit-Zagardo (Gruber et al., 2014). Mice were originally described by Angelillo-Scherre and colleagues (Angelillo-Scherrer et al., 2001). Age and sex-matched *C57BL/6* femurs (Jackson Laboratory) were used as controls (n = 6 bones). Bone marrow from Gas6$^{-/-}$ and age and sex-matched *C57BL/6* femurs were processed in the same fashion, and transplanted into n = 10 seven-week old female *C57BL/6* mice (n = 5 per condition). Mice were maintained in sterile conditions in the Animal Facility for two months before nerve injury, then another two weeks after nerve injury.

Human Nerve Injury

Three patient samples were used for human nerve tissue analysis. The region distal to the nerve injury, where widespread macrophage accumulation was apparent, was processed for immunohistochemical analysis. This included: A blunt stretch nerve injury (axillary nerve, 20 weeks post-injury, male, 32 years old); glass laceration nerve injury (ulnar nerve, 11 days post-injury, male, 31 years old); and a stretch nerve injury (axillary nerve, 23 weeks post-injury, female, 71 years old).

Adult primary Schwann cells and conditioned media

Schwann cells and conditioned media were obtained from cells derived from 4-8 healthy uninjured 6-8-week-old *C57BL/6* female mice.

METHOD DETAILS

Bone marrow transplants

The recipient rats were lethally irradiated with a dosing schedule of 2 × 5.5 Gy, 4 hours apart using a gamma irradiator with a caesium-137 source (Gammacell 40; Best Theratronics). Donors were euthanized with CO_2 and the femurs isolated on ice. The bone marrow was flushed from the femurs with 10mL of HBSS and then centrifuged for 15 min at 300 g. The red blood cells were lysed and bone marrow cells resuspended at 5x10^7 bone marrow cells/mL in HBSS. 200 μL (10x10^6 bone marrow cells) were injected via the tail vein of prepared recipients under light anesthetic. The success of the transplant was assessed after 6 weeks and animals with greater than 70% GFP$^+$ white blood cells (as assessed under epi-fluorescent microscopy) were used for experimentation at eight weeks post-transplant.

Rodent nerve injuries

All surgeries and electrophysiological readings were carried out under isoflurane (2%–5%) inhalation anesthetic with postoperative pain control provided by subcutaneous injections of buprenorphine (0.05 mg/kg) on the day of surgery for both rat and mouse experiments, followed by oral administration of buprenorphine (0.03 mg/kg) for rats and subcutaneous injections for mice on the days following. All surgical and electrophysiological procedures were carried out following the shaving of the hind limb area in an aseptic fashion using 70% ethanol. Under operating microscopes (M651, Leica), sciatic nerves were exposed at the sciatic notch and crushed for 10-20 s using bevelled Dumont No. 5 forceps (L4¼inch, Inox alloy, Sigma).

Macrophage ablation and CMAPs

For ablation experiments, at 8 days post-nerve injury, the distal nerves of 9 animals received an intraneural injection (5 μl) of mannosylated liposomes (8907, Clodrosome) encapsulating either clodronate (dichloromethylene diphosphonate; Cl2MDP, n = 3), PBS (n = 3) or fluorescent lipids (n = 3) as previously described (Miron et al., 2013). Liposomes were delivered over a 10 s period using a 30-gauge Hamilton syringe. Tissue was then collected for immunohistochemical analysis at 18 days post-nerve injury – a time point where substantial remyelination in young healthy rodents has usually occurred (Lim et al., 2017). For electrophysiological analysis, at 6-8 days post-nerve injury animals received an intravenous injection (200 μl) of mannosylated liposomes (8907, Clodrosome) encapsulating either clodronate (dichloromethylene diphosphonate; Cl2MDP, n = 4) or PBS control (n = 3) (Kubota and Suzuki, 2000). Electrophysiological measurements were recorded as previously reported (Lim et al., 2017). Compound muscle action potential (CMAP) amplitudes were measured in contralateral nerves and 6 weeks post injury and the average value from three measurements at the same stimulation site was recorded. The body temperature of animals was kept constant at 37°C ± 0.5°C throughout the experiment on a heating pad. Motor latencies and conduction velocity (CV) measurements were also recorded. For normalized distal motor latencies, the sciatic nerve was stimulated just above the sciatic notch and the knee (popliteal fossa) using bipolar hook electrodes and the electromyogram activity was recorded (100 × ; 100 Hz to 1 kHz) using bipolar recording electrodes inserted into the first dorsal interosseous muscle of the corresponding hind limb. The experimenter was blinded to the post-injury time during recording. Conduction velocity was then calculated by dividing the difference in distance between the knee and the sciatic notch stimulating sites by the difference in the latencies of the respective CMAPs.

Immunohistochemistry and *in situ* hybridization

Before tissue collection, mice were euthanized with an overdose of sodium pentobarbital or isoflorane followed by cervical dislocation. Dissected nerves were post-fixed in 4% PFA at 4°C overnight and subsequently allowed to equilibrate in 30% sucrose at 4°C overnight, before finally embedding in cryoprotectant (VWR Clear Frozen Section Compound) for storage at −80°C. Sciatic nerve segments stretching from 2 mm proximal to 1cm distal from the crush site was collected. Twelve micron thick longitudinal sections were cut and stored at −80°C. Two to three high-quality sections per nerve per condition were selected for immunohistochemistry. Briefly, sections were permeabilized and blocked in 0.3% triton and 5% BSA (1 hour at room temperature) before primary antibody incubation overnight at room temperature. Immunostains were using anti- ionized calcium-binding adaptor molecule 1 (Iba1, rabbit, 019-19741, Wako, 1:200), anti-Cx3cr1 (rabbit, TP501, Torrey Pines Biolabs Inc, 1:500), anti-CD68 (mouse, MCA341R, Biorad, 1:200), anti-Ly6C (APC-conjugated, clone AL-21, BD Biosciences, 1:50), anti-CD206 (goat, AF2535, R&D, 1:200), anti-P0 (Po anti-peptide antibody cocktail, PZ0, Aves lab, 1:200), anti-Ki67 (rat, 14-5698-82, ThermoFisher, 1:200), anti-Sox2 (goat, Santa Cruz, sc-17320), anti-Sox10 (goat, Santa Cruz, sc-17343, 1:200), anti-HBEGF (goat, AF259NA, R&D, 1:100), anti-Gas6 (rabbit, sc22759, Santa Cruz, 1:100), anti-IL6 (goat, af506, R&D, 1:100), anti-s100 (rabbit, Z0311, Dako, 1:500) and anti-Thy1 (mouse, MMS-435P, Covance, 1:500). After washing, cells were incubated at room temperature for 1-2 h with secondary antibodies conjugated to either Alexa Fluor 488, 555 or 647 (donkey anti-mouse, rabbit, rat, goat, 1:200, Invitrogen), Hoechst-33258 (1:1000, 14530, Sigma) and in some instances Fluormyelin (Invitrogen), then washed and coverslipped. All immunohistochemical stains were confirmed positive with appropriate no primary (secondary alone) controls. Image collection and quantification was done using either Nikon A1 or a Leica SP8 confocal microscope. Whole nerve montage was collected using a 20x objective lens, Tile-Scan and Z stack (8 z-planes) features, and maximum projection images. For all other images, sections were imaged at 63x objective, 10-20 serial z stacks in 0.5 μm - 1.0 μm steps, then usually maximum projected before quantifying. For myelin analysis, orthogonal view features were used to scroll through z stacks to determine the z-plane containing the widest gap between parallel myelin profiles from a given Schwann cell. Myelin thickness was measured on LAS-AF (Leica) by placing a measure line perpendicular to a given myelin profile starting from the myelin closest to where the axolemma sits, through the myelin, to the outer most point of myelin within a given profile. This is a validated method where outcomes are equivalent to electron microscopy analysis (Mirfeizi et al., 2017; Oluich et al., 2012). For segment length a similar approach was taken but images were first maximally projected before placing the measure line along the length of the myelin segment. Importantly, the images were consistently imaged across groups with narrow increments of z stacks in order to obtain the large majority of each internode that was present within a given section. Four to five images per animal were collected at proximal end, 0.0 mm, 1.0 mm, 2.0 mm, and 3.0 mm from crush site (for mouse); or proximal end, 0.0 mm, 2.5 mm, 5.0 mm, and 7.5 mm (for rat) from crush site. All imaging of a given stain was performed using the same laser settings. We used ImageJ and designated markers to count cells or cellular components of interest, as well as nuclear stains. All quantification was done while blinded.

For human nerve tissue analysis, samples were formalin-fixed, paraffin embedded, and sectioned at 5 μm. Deparaffinization was performed using 2x 5-10 min Xylene, 2x 5-10 min 100% ethanol, 1x 5 min 95% ethanol. Antigen retrieval was performed using 10mM Sodium Citrate for 30 minutes at 100°C. Immunohistochemistry was then performed using the antibodies and approach outlined above (+ anti-p75, G323A, Promega, 1:200). For *in situ* hybridization, we used an RNAscope singleplex assay (Advanced Cell Diagnostics). The RNAscope probes targeting human growth arrest-specific 6 (GAS6) contain 20 double Z oligonucleotide primers (18-25 base pairs) against the GAS6 coding region (NM_000820.3, Cat#427811). The probe used as a negative control targets the non-specific bacterial dihydrodipicolinate reductase (dapB) gene, which is not expressed in mammalian tissues, was negative. The double Z target probe system of RNAscope technology allows each probe to reliably detect RNA at single molecule resolution, while preventing amplification of non-specific signals. The probe is magnified by branching amplification and then developed using an alkaline phosphatase reaction with the Fast Red substrate. Briefly, sections were processed following the standard RNAscope singleplex protocol. Sections were first deparaffinised, as above, then boiled in target retrieval solution for 15 min to facilitate heat-induced epitope retrieval, and subsequently permeabilized with a broad-spectrum protease for 30 min. Samples were then hybridized with target-specific probes for 2 h at 40°C, washed, then hybridized with amplifiers and visualized using the Fast Red substrate via alkaline phosphatase reaction. Immediately after, slides were processed for immunohistochemistry as above.

In vitro Schwann cell experiments

Following euthanasia of 4 adult *C57BL/6* mice (using an overdose of sodium pentobarbital/severing the cervical spinal cord), sciatic nerves were isolated, sterilized and cleared of hair, membranes and connective tissue (Stratton et al., 2017). Samples were finely chopped using a sterile blade, then put in collagenase (2 mg/ml, Worthington, Lakewood, NJ, USA) at 37°C for 30-40 minutes, triturating every 10-15 minutes until solutions appeared cloudy, then filtered with a 70 μm filter. Samples were centrifuged for 5 minutes at 200G, supernatant discarded, then resuspended in media. Medium was composed of neuregulin (50 ng/ml, R&D), forskolin (5 μM, Sigma), N2 supplement (1%, Invitrogen) and penicillin/streptomycin (1%, Invitrogen) in DMEM/F12 (3:1, Invitrogen) herein referred to as Schwann cell media. Plating substrate was PDL/laminin (BD Biosciences). Up to 5% FBS was used during initial establishment of our Schwann cell cultures. All cells had media changes every 3-4 days and were maintained in humidified incubators at 5% $C0_2$ and 37°C. Cells were used for experimentation at passage 2-5. For Schwann cell conditioned media collections, cells were first plated at 50,000 cells/ml in 10 cm plates, then once cells had reached 80% confluence, 10 mL of fresh Schwan cell media was added. Five

days later, once cultures had reached 100% confluence (~3 million cells), media was collected, filtered (0.2 μm), then placed at −80°C. In parallel, for media alone controls, 10 mL of Schwann cell media was plated in 10 cm plates without cells and then collected in the same fashion.

To obtain conditioned media from macrophages and fibroblasts, first adult mice (n = 4-6 per cell type) were euthanized (using an overdose of sodium pentobarbital/ severing the cervical spinal cord). Mice were sterilized and cleared of hair and skin. For fibroblast collections, the same procedures as described above were used except 10% fetal bovine serum rather than neuregulin and forskolin was added to media. Within 2 week of plating, the cultures were primarily composed of fibroblasts. For conditioned media collections, fibroblasts were first plated at 50,000 cells/ml in 10 cm plates, then once cells had reached 80% confluence, 10 mL of fresh media was added. Five days later, once cultures had reached 100% confluence (~3 million cells), media was collected, filtered (0.2 μm), then placed at −80°C. In parallel, for media alone controls, 10 mL of media was plated in 10 cm plates without cells and then collected in the same fashion. For macrophages, femurs were obtained, and then cells from bone marrow were collected by flushing 5 times with ice-cold calcium and magnesium-free PBS. Samples were centrifuged for 5 minutes at 200 G, supernatant discarded, then resuspended in media and plated at 500,000 cells/ml. Media included 100 ng/ml recombinant M-CSF (R&D systems), 1% Pen Strep (GIBCO), 2% MEM non-essential amino acid solution (GIBCO) and 10% fetal bovine serum (Sigma-Aldrich) in DMEM. The day after plating, once cells had settled, media was changed. Once cells had reached 80% confluence (~5 days post plating), media was changed, 10 mL of fresh macrophage media was added. Four-five days later, once cultures had reached 100% confluence (~3 million cells), media was collected, filtered (0.2 μm), then immediately used or placed at −80°C. In parallel, for media controls, 10 mL of macrophage media was plated in 10 cm plates without cells and then collected in the same fashion.

For all *in vitro* experiments out-lined in this manuscript, cells were plated at 50,000 cells/ml in 96 well plates, initially in Schwann cell media (ie. under proliferative conditions). At 12 hours post-plating, media was removed, then cells were treated with either conditioned media from Schwann cells, macrophages, fibroblasts, depleted media or recombinant proteins including HBEGF (100-47, Peprotec); Gas6 (CF 885-GSB-050, R&D); and IL6 (506-RL-010, R&D) diluted in DMEM. Forty-eight hours later, cells were fixed in 4% paraformaldehyde for 5-10 minutes and stored in PBS at 4°C for up to 1 week before immunocytochemical processing. In preparation for antibody incubation, cells were blocked and permeabilised for 1-2 h at room temperature in 5% BSA and 0.5% Triton X-100. Cells were then incubated overnight at 4°C with a polyclonal antibody: anti-S100β (rabbit, Dako, Z0311, 1:200), anti-O4 (FITC-conjugated, MAB345A4 Millipore, 1:50), anti-Ki67 (rat, 14-5698-82, ThermoFisher), anti-P0 (Po anti-peptide antibody cocktail, PZ0, Aves lab, 1:200), anti-Sox10 (goat, Santa Cruz, sc-17343, 1:200). After washing, cells were incubated at room temperature for 1-2 h with secondary antibodies conjugated to either Alexa Fluor 488, 555 or 647 (donkey anti-mouse, rabbit, rat, goat, 1:200, Invitrogen) and Hoechst-33258 (1:1000, 14530, Sigma). Stained Schwann cells were imaged and quantified using an ImageXpress Microscrope (Molecular Devices). For all *in vitro* immunocytochemical experiments, each condition consisted of 3-4 replicates, with statistical analyses performed on the averaged value from 12 images per replicate. Each cell culture experiment (3-4 replicates per condition per experiment) was replicated on two-four independent days with the representative experiments presented in this paper being accurate reflections of findings across multiple experiments.

Macrophage FACs isolations & RNaseq

At Day 3 and 8 post-nerve injury, *Cx3cr1*-GFP$^+$ *Ccr2*-RFP$^+$ double positive cells were FACS collected from *Cx3cr1*-GFP/*Ccr2*-RFP mice. Following euthanasia of 16 mice (8 per time point) using $C0_2$ affixation and severing the cervical spinal cord, sciatic nerves were isolated, sterilized and cleared of hair, membranes and connective tissue. Blood was also collected and mixed with sodium-EDTA (10% w/v in water), then centrifuged before collecting the buffy coat (containing white blood cells). Red blood cells were lysed using water (for 30 s), before sample being re-suspended in 0.5% BSA in HBSS for FACS purification. Nerves were finely chopped using a sterile blade, then put in collagenase (2 mg/ml, Worthington, Lakewood, NJ, USA) at 37°C for 30 minutes, triturating every 10 minutes until solutions appeared cloudy, then filtered with a 70 μm filter. Samples were centrifuged for 5 minutes at 200 G, supernatant discarded, then re-suspended in 0.5% BSA in HBSS before FACS purification using a BD FACS Aria machine. A stringent initial gate was used to exclude debris and cell doublets. Wild-type cells were used as negative controls to determine gates for detecting GFP and RFP, and then macrophages were purified according to these gates. The number of cells collected from each animal is listed: Day 3 - 19,041; 13,548; 23,989; 17,242; 13,502; 19,901; 8,472; 11,194; Day 8 - 16,343; 19,667; 8,538; 7,312; 10,411; 11,880; 12,198, 4,460; Blood – 16,581; 11,699; 5,495; 27,154; 39,526; 27,392; 49,369; 9,169. Due to low levels of RNA, samples were pooled so 2 samples per condition were analyzed. All cells were sorted directly into lysis buffer (Ambion), then triturated and vortexed before storage at −80°C. For RNA extractions, all samples were processed together following manufacturers recommendations (AM1561, Ambion). Total RNA extracts were quantitated using a Qubit Fluorimeter and the Qubit HS assay kit (Invitrogen). All samples were subjected to reverse transcription and Multiple Displacement Amplification (MDA) with REPLI-g SensiPhi DNA Polymerase and oligo-dT primers as per the QIAGEN REPLI-g Single Cell RNA Library preparation kit (150073) and the manufacturer's protocol. The amplified cDNA produced was then sheared to an average 300 bp using a Covaris S220 sonicator and Covaris microtubes with AFA fibers (520045). Illumina compatible libraries were then prepared using the QIAGEN GeneRead Adaptor I Set A 12-plex (180985) index adapters as per the REPLI-g single cell RNA library prep kit's protocol. Products were quantitated and sized using both a Qubit fluorimeter with QuantiFluor dsDNA System dye (Promega E2670) and an Agilent 2200 TapeStation with D1000 ScreenTape and reagents (5067-5583). 500-600 ng of the final library were obtained from each sample. Each library was quantitated using the Kapa qPCR Library Quantitation Kit for Illumina (KK4835) on a StepOne Plus qPCR instrument prior to preparing a single pool containing

equal amounts of each library. This pool was then subjected to on-board cluster formation and sequencing on an Illumina NextSeq 500 sequencer with a high-output v2 75 cycle sequencing kit (FC-404-2005) as per the standard Illumina protocols. After sequencing, the bcl data was converted to fastq data files using the Illumina BCL2FASTQ utility. The sequencing run produced 475 million clusters passing filter (density = 206 K/mm2) and 34.8 gigabases of sequencing with quality scores of > = Q30 (91.4%). The number of assigned reads for each sample was between 39.1 million and 43.9 million.

RNaseq bioinformatics

Alignment was performed using bwa 0.7.12 in ''mem'' alignment mode against mm10 reference genome with default parameters. Transcription quantification, differential expression analysis, and heatmap creation were performed in the R programming language using GenomicAlignments, Pheatmap, and DESeq2 (Lawrence et al., 2013, Love et al., 2014). Expression was summarized at the gene level using the ''union'' mode of summarize overlaps. A false discovery rate corrected p value of 0.05 for the Wald test was used for linear model of factors. Output was imported into Ingenuity Pathway Analysis (IPA) software for VENN diagram, physiological function analysis, and cellular component assignment.

Flow cytometry to detect intracellular cytokines

To evaluate the expression ligands in macrophages following nerve injury, nerves from *Cx3cr1*-GFP/*Ccr2*-RFP mice were processed into single cell suspensions and then prepared for flow cytometry (Jung et al., 1993). Nerves were first extracted and processed in the same fashion as mice used in the RNaseq experiment. The single-cell suspension was then centrifuged at 1000 rpm for 5 minutes, then washed twice with a large volume of PBS, and fixed in 1% PFA. Cells were then blocked and permeablized with 0.5% Saponin, 1% BSA, and rat anti-CD16/32 (1:200, Mouse BD Fc Block, BD Biosciences) for 30 min at room temperature. Cells were then incubated with anti-HBEGF (goat, AF259NA, R&D, 1:100), anti-Gas6 (rabbit, sc22759, Santa Cruz, 1:100), or anti-IL6 (goat, af506, R&D, 1:100) antibodies for 1 hour, then resuspended in PBS and washed. A subset of cells from each sample was treated identically, but no primary antibody was added. Secondary antibodies (donkey anti-goat or rabbit 647, Invitrogen) were added for 30 minutes then washed twice. Samples were run on a BD FACS Aria machine with FACSDiva software (BD Biosciences) and analysis was performed using FlowJo software.

QUANTIFICATION AND STATISTICAL ANALYSIS

For comparisons of groups across multiple groups, a one-way analysis of variance (ANOVA) followed by Tukey's post hoc comparison was used (GraphPad Prism 5). For comparisons of groups across 2 groups, an unpaired Student t test was used. For comparisons of multiple factors across 2 groups, multiple unpaired Student t tests with a false discovery rate of 5% were used. *P value*s < 0.05 was considered significant. All other statistical details can be found in figure legends and methods section.

DATA AND SOFTWARE AVAILABILITY

The accession number for the RNAseq data reported in this paper is GEO: GSE106927.